Optimal Allocation of Dynamic Var Sources Using the Voronoi Diagram Method Integrating Linear Programing

Weihong Huang, *Student Member, IEEE*, Kai Sun, *Senior Member, IEEE,* Junjian Qi, *Member, IEEE,* and Jiaxin Ning, *Member, IEEE*

***Abstract*—Dynamic reactive power (var) sources can effectively mitigate fault-induced delayed voltage recovery (FIDVR) issues. This paper optimizes the sizes of dynamic var sources at given locations against FIDVR issues under severe contingencies. First, the geometric characteristics about the non-convex solution space of this problem are studied. Accordingly, a Voronoi diagram approach integrating linear programming (LP) is proposed, which disperses a number of sample points of potential solutions in the searching space to construct a Voronoi diagram blending the local cost functions over the entire space by Barycentric interpolation in Voronoi regions. New sample points are then recursively added, including the tentative optimal point using LP, the most depopulated area point ensuring global fidelity, and the connecting point, until the stopping criterion is met. The new approach is demonstrated in detail on the WSCC 9-bus system. A case study on the NPCC 140-bus system also validates that the proposed approach can effectively estimate the boundary and the geometry of the feasible solution region in the searching space and find the optimal solution.**

***Index Terms*--Barycentric interpolation, dynamic var support, fault-induced delayed voltage recovery, FIDVR, linear programming, nonlinear optimization, Voronoi Diagram.**

I. Introduction

In recent years, fault-induced delayed voltage recovery (FIDVR) issues have drawn growing attentions, especially in the areas with a lot of air conditioning loads. In order to economically guarantee voltage security and prevent FIDVR issues, it is important to optimally allocate and manage dynamic var sources such as static var compensators (SVCs) and STATCOMs.

The optimal allocation of dynamic var sources has been studied in [1]–[13] and needs to address two problems, i.e. the optimal placement and optimal sizing of var sources, which are usually solved separately. The optimal placement problem is traditionally solved by calculating a voltage sensitivity index for each candidate location so as to identify where an injection of dynamic var can improve post-fault voltage recovery to the largest extent for the most severe one or multiple contingencies [3]–[5]. A recent work applies the empirical controllability covariance to place dynamic var sources which can reduce the dependency on the selection of contingencies [6].

In existing studies, the optimal sizing problem of the dynamic var sources is usually formulated as a mixed integer programming problem and addressed by interfacing a heuristic optimization algorithm with power system simulation. In [7], the dynamic var allocation problem is formulated as a mixed integer nonlinear programming problem and solved by interfacing the branch-and-bound and multi-start scatter algorithms, which are available in MATLAB with power system time-domain simulation software. A similar problem is solved in [8] by interfacing a MATLAB-based toolbox KNITRO with power system simulation. In [9], the sizing of dynamic var sources is optimized by a multi-objective evolutionary algorithm called MOEA/D. The approach presented in [10] employs the mean-variance mapping optimization in combination with an integrated mix-integer search strategy and two intervention schemes for a number of most severe "N-1" contingencies. In [11] the optimal locations and amounts of static and dynamic var sources are solved as a sequence of mixed integer programming problems. The particle swarm optimization method is applied in [12] for the installation of dynamic var sources including wind farms. In [13] a heuristic linear programming method is proposed for a small number of dynamic var sources.

Our previous work in [14] has tentatively shown that Voronoi diagram, as an effective technique for generating contour map [15], can approximate the geometry of the solution space of the problem very well. This paper aims to tackle the optimal sizing of dynamic var sources from a new perspective: first, a study on the geometric characteristics about the solution space indicates the non-convexity of the feasible solution region and relative flatness near the optimal solution; accordingly, the Voronoi diagram method integrating linear programming (LP) is proposed to effectively find the optimal solution.

W. Huang, and K. Sun are with the Department of Electrical Engineering and Computer Science, University of Tennessee, Knoxville, TN, 37996 USA (e-mails: whuang12@vols.utk.edu; kaisun@utk.edu)

J. Qi is with the Energy Systems Division, Argonne National Laboratory, Argonne, IL 60439 USA (e-mail: jqi@anl.gov).

J. Ning is with the Dominion Virginia Power, Richmond, VA, USA (e-mail: Jiaxin.Ning@dom.com).

The rest of this paper is organized as follows. Section II discusses the formulation of the problem. Section III analyzes the general geometric properties of the feasible solution region in the solution space. Section IV introduces the Voronoi diagram based blending of local function expression. Section V proposes the new approach using the Voronoi diagram method integrating LP. Then in Section VI, the proposed approach is illustrated in detail on WSCC 9-bus system and then validated on the NPCC 140-bus system. Finally, conclusions are drawn in Section VII.

II. Formulation of the Problem

The optimal allocation problems of dynamic var sources can be formulated based on industry practices. To address FIDVR issues, power companies follow certain reliability standards to determine the locations and sizes of dynamic var sources for reducing voltage deviations under a contingency [16]. Consider an N-bus power system to place dynamic var sources against potential FIDVR issues under K selected contingencies. The percentage voltage deviation of a bus j at time t under the k-th contingency can be defined as:

$$r_j^k(t)=\left|\frac{V_j^k(t)-V_j^{init}}{V_j^{init}}\right|\times 100\% \quad j=1,\cdots,N,\ \ k=1,\cdots,K \tag{1}$$

where V_j^{init} is the pre-fault voltage magnitude. The fault clearing time is denoted by t_{cl} and the post-fault transient period is defined to be t_s after t_{cl}. Without losing generality, this paper considers the following constraints C_1 to C_3 on the post-fault transient voltage performance:

- C_1: $r_j^k(t)\le \mathrm{R}_1$ for $t_{cl}\le t\le t_s$.
- C_2: The duration for $r_j^k(t)$ exceeding $\mathrm{R}_2\le \mathrm{D}$ for $t_{cl}\le t\le t_s$.
- C_3: $r_j^k(t)\le \mathrm{R}_3$ for $t>t_s$.

Typical parameters based on the WECC/NERC standards [17] are considered in this paper: R_1=25% for load buses and 30% for generator buses; R_2=20% and D=1/3 second; t_s=3 seconds and R_3=5%. Fig. 1 illustrates the criteria for a load bus.

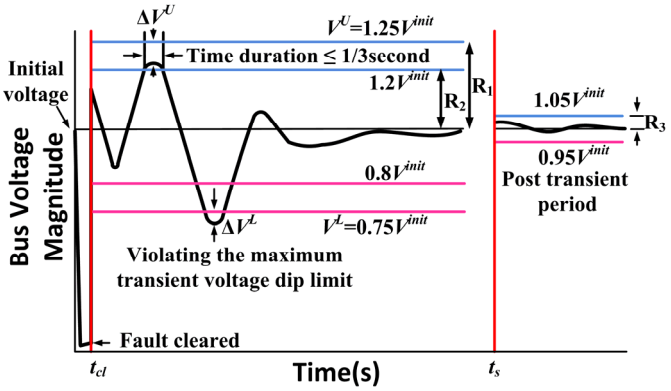

Fig. 1. Post-fault voltage performance criteria for a load bus.

Within a given post-contingency period, check constraints C_1 to C_3 for T time points at intervals of Δt (e.g. 4.167 ms). Define a severity index $S_j^k(\tau)$ for bus j under contingency k at the τ-th time point of the period, which equals $r_j^k(\tau\times\Delta t)$ if any constraint is violated, or 0, otherwise. Then, for contingency k, the average severity index S^k for the overall system and all time points of the period is calculated as

$$S^k=\frac{1}{T\cdot N}\sum_{j=1}^{N}\sum_{\tau=1}^{T}S_j^k(\tau)\,. \tag{2}$$

Assume that the buses to install dynamic var sources have been determined by power system planners using an optimal placement approach as well as engineering judgement giving considerations to factors on system operations. The index set of those selected buses is denoted by $\mathrm{I_Q}$. The optimal sizing problem can be formulated as:

$$\text{Minimize } J_1=\mathbf{c}^{\mathrm{T}}\mathbf{Q} \tag{3}$$

Subject to

$$\dot{\mathbf{x}}=\mathbf{f}(\mathbf{x},\mathbf{V},\mathbf{Q}) \tag{4}$$

$$\mathbf{0}=\mathbf{g}(\mathbf{x},\mathbf{V},\mathbf{Q}) \tag{5}$$

$$\mathbf{Q}^{\mathrm{L}}\le\mathbf{Q}\le\mathbf{Q}^{\mathrm{U}} \tag{6}$$

$$C_1,\ C_2 \text{ and } C_3 \tag{7}$$

where $\mathbf{Q}=[Q_1,\ \ldots,\ Q_N]^{\mathrm{T}}$ is a column vector about the sizes of dynamic var sources installed at N buses, whose upper and lower limits are respectively in vectors $\mathbf{Q}^{\mathrm{U}}$ and $\mathbf{Q}^{\mathrm{L}}$, and there is $Q_i\equiv Q_i^U\equiv Q_i^L\equiv 0$ if $i\notin \mathrm{I_Q}$; and $\mathbf{c}=[c_1,\ \ldots,\ c_N]^{\mathrm{T}}$ is the column vector of costs per Mvar (e.g. the installation and maintenance costs) associated with the dynamic var sources. The objective is to find the optimal vector $\mathbf{Q}$ so as to minimize the objective function J_1 under all constraints. In practice, with the post-fault voltage trajectories obtained from time-domain simulation, the constraints C_1 to C_3 can be checked at each simulation step Δt.

In general, the set of feasible solutions of the optimization problem in (3)–(7) is non-convex. Also, the optimization is coupled with resolution of power system differential-algebraic equations (DAEs) in (4)–(5) for post-fault system trajectories, which dramatically increases the computational complexity. Taking exhaustive search as an example, post-fault voltage responses need to be first solved for all contingencies with each possible $\mathbf{Q}$, based on which the voltage criteria C_1 to C_3 need to be checked. Only when all responses satisfy the criteria, such a vector $\mathbf{Q}$ indicates a feasible solution. After all possible feasible solutions are found, the optimal $\mathbf{Q}$ can then be obtained as the final solution.

III. Geometry of the Solution Space

To integrate C_1, C_2, and C_3 into the cost function, the objective function J_1 is modified as

$$J_2=\mathbf{c}^{\mathrm{T}}\mathbf{Q}+c_p\sum_{k=1}^{K}b_k \tag{8}$$

where binary variable b_k equals 1 if the k-th contingency makes any constraint violated or equals 0, otherwise, and $c_p>>c_i$ is the penalty of voltage violation. Next, the geometry of the solution space about the objective function (8) is studied in order to develop an effective algorithm for this optimization problem.

As an example, the WSCC 3-generator 9-bus system shown in Fig. 2 is studied. The most severe "N-1" contingency is identified as the three-phase fault at bus 7 cleared by opening

line 5-7 after 5 cycles. Here, set c_i=\$1,000/Mvar, c_p=\$300,000 and Q_i^L=0 Mvar. The solution spaces for installing one SVC at bus 6 and three SVCs at all of three load buses are obtained by exhaustive search in the range of [0, 85] (Mvar) for each Q_i, from which some useful insight can be gained on geometric characteristics of the solution space.

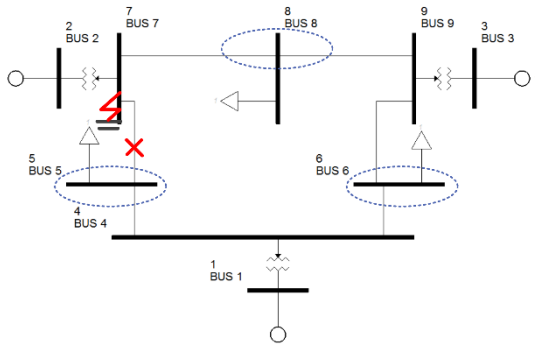

Fig. 2. The most severe N-1 contingency of WSCC 9-bus system and three candidate buses for dynamic var supports.

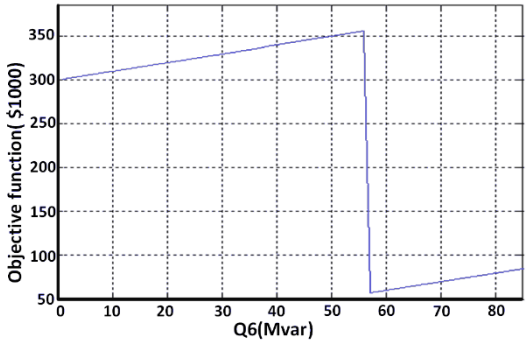

Fig. 3. One SVC size at bus 6 and its corresponding objective function.

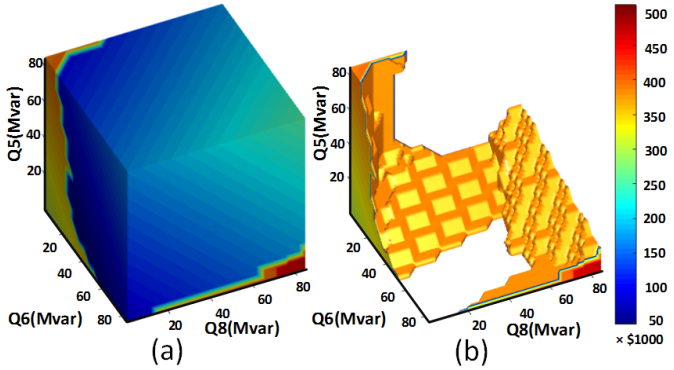

Fig. 4. The contour map of objective function and its infeasible solution space.

First, consider installing one SVC at bus 6. Fig. 3 depicts how the objective function changes with the size of the SVC, which is basically piece-wise linear and has the minimum at Q_6=57 Mvar, which is right at a joint of two linear segments.

For installing three SVCs at buses 5, 6, and 8, the contour map about the cost function varying with the sizes of three SVCs is shown as Fig. 4(a), where the colder the color, the smaller value the objective function has. In fact, the feasible solutions of the original problem defined in (3)–(7) correspond to J_2≤\$285,000. Fig. 4(b) visualizes the infeasible solutions and the boundary of the feasible solutions.

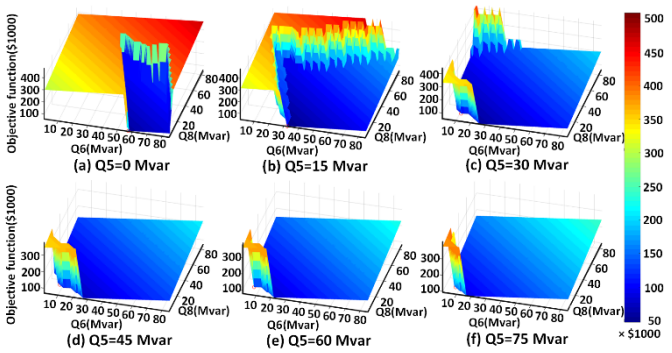

Fig. 5. Contour map of objective function when the SVC of bus 5 is fixed.

To better understand the geometry of the region of feasible solutions, let Q_5 respectively take a value from {0, 15, 30, 45, 60, 75} each time and the objective function J_2 is evaluated for all combinations of Q_6 and Q_8. The contour maps about the cost function are shown in Fig. 5. For different values of Q_5, the following are observed:

- When Q_6 and Q_8 increase starting from an infeasible solution, J_2 first increases almost linearly and then sharply drops to a small value when the penalty is no more applied, or in other words, when the solution becomes feasible.
- The feasible solution region is relatively flat, in which J_2 basically increases in a linear manner.
- The optimal solution (darkest blue) appears close to the boundary of the feasible solutions.
- The boundary of the feasible solutions is not smooth.

These observations coincide with the characteristics of Fig. 3 for installing one SVC.

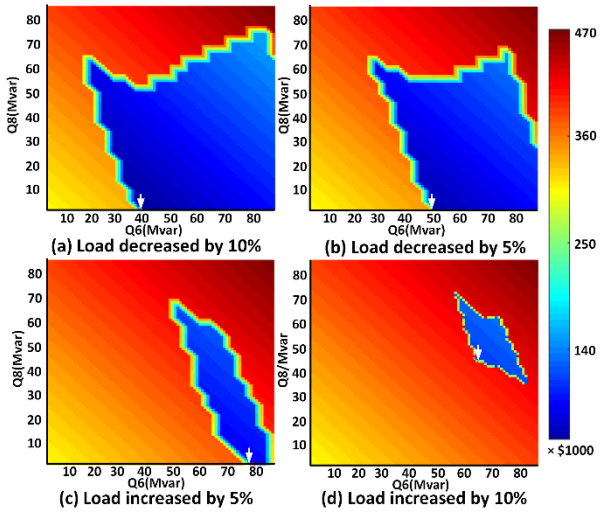

Fig. 6. The contour maps of the objective function, where the region (blue) of feasible solutions are shown under four different loading conditions.

Furthermore, the impacts of load and generation variations are investigated. Specifically, we change the system load together with the total generation by -10%, -5%, +5%, and +10%. For these four new loading conditions, the contour maps about the objective function are shown in Fig. 6. Each blue area indicates the region of feasible solutions, which

shrinks with the increase of the load. The global optimum also moves as indicated by the white arrow. Despite the change of load, the aforementioned four observations are still valid with these contour maps. Another important observation is that the optimum for a heavy-load condition (e.g. the +10% load increase case) is still in the feasible region for a light-load condition.

When the objective function J_2 is used, because of the high penalties added to voltage violations in (8), the above geometric characteristics may be generalized for the optimal sizing problem of dynamic var sources. Thus, it is reasonable to make use of these geometric characteristics of the solution space and design an effective algorithm to solve the problem. An idea is to first approximately depict the boundary and geometry of the feasible solution region, which corresponds to the blue region in Figs. 4–6, and then attempt to find the optimal solution only in that region so that simple and fast optimization techniques like LP can be adopted.

In the next two sections, the Voronoi diagram and the Barycentric interpolation will be introduced as an efficient technique for geometric and function approximation, and a new approach based on the Voronoi diagram method integrating LP will be proposed to effectively solve the optimal sizing problem of dynamic var sources.

IV. Voronoi Diagram Based Blending of Local Function Approximation

This section introduces the fundamentals of Voronoi diagram and Barycentric interpolation. In literature, Voronoi diagram based blending methods of local response surfaces have been proposed to accomplish global fidelity in function approximation for engineering designing optimization [18].

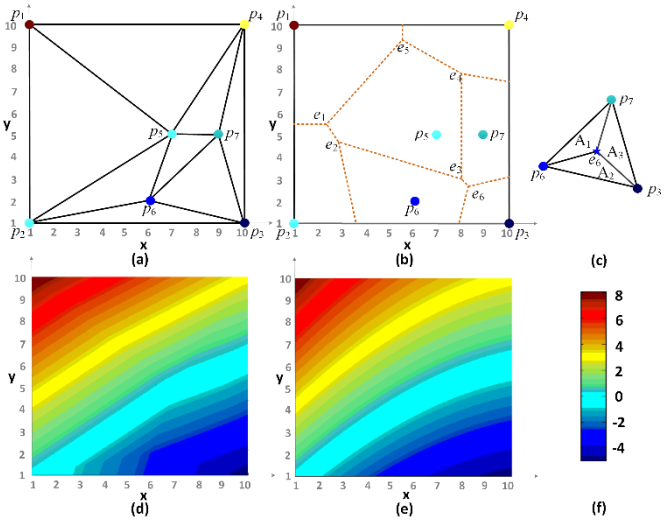

Fig. 7. Generating Voronoi diagram and local function estimation.

A Voronoi diagram based Barycentric interpolation can estimate the boundary and geometry of the feasible solution region in any dimension. Voronoi diagram partitions a plane into regions based on the distance to the sample points and can provide geometric information of sample points, such as the most depopulated area in the plane. Barycentric interpolation can estimate the local function expression around sample points in each small Voronoi region.

The following example illustrates the essence of Voronoi diagram and Barycentric interpolation in a two dimensional plane x-y. The searching range is [1, 10] for both x and y, and the function of x and y is $z=x^2/25-y^2/100-x+y$. To estimate the function values over the entire plane, the values at a sample point set P=$\{p_1, p_2,..., p_7\}$ including 4 searching boundary points and 3 distinct random points are first calculated and colored by their values as shown in Fig. 7(a). Perpendicular bisectors are drawn for each pair of the distinct points in P. These result in a set of polyhedra (polygons for this 2-D case) as illustrated by orange dash lines in Fig. 7(b). This is called a Voronoi diagram denoted as *Vor(*P*)*. The cell of *Vor(*P*)* that corresponds to a site p_i is called a Voronoi region of p_i denoted by $Vor(p_i)$. All of the intersection points such as e_1, e_2, ... are called Voronoi points. Taking p_5 as an example, its Voronoi region, $Vor(p_5)$, is composited by Voronoi points $e_1e_2e_3e_4e_5$. Denote the Euclidean distance between any two points p and e by $dis(p,e)=\sqrt{(p_x-e_x)^2+(p_y-e_y)^2}$. The judge of the territory of each Voronoi region, any point a lies in $Vor(p_i)$ if and only if $dis(a, p_i)<dis(a, p_j)$ for any $p_j \in$ P with $j \neq i$.

As illustrated in Fig. 7(b), since p_3 has a smallest function value, so $Vor(p_3)$ is most likely to contain the minimum value. To estimate the function values inside this region, Barycentric interpolation is applied to estimate local function values in triangles about any three adjacent p points. Taking triangle $p_3p_7p_6$ for example, each point located inside this triangle can be written as a unique convex combination of the three vertices. To estimate the function value of an inside point e_6 as shown in Fig. 7(c), a unique sequence of three positive numbers, a_1, a_2, and a_3, can be found such that $a_1+a_2+a_3=1$ and $e_6=a_1p_3+a_2p_7+a_3p_6$. Here a_1, a_2, and a_3 are the Barycentric coordinates of the point e_6 with respect to the triangle and there are $a_1=A_1/(A_1+A_2+A_3)$, $a_2=A_2/(A_1+A_2+A_3)$ and $a_3=A_3/(A_1+A_2+A_3)$, where A_1, A_2, A_3 are the sub triangle areas shown as in Fig. 7(c). Each point inside $p_3p_7p_6$ is uniquely defined by any two of the Barycentric coordinates. Finally, e_6 is colored with its corresponding value as an estimate of the function value there.

With the 7 points in the plane, the entire space can be estimated by Barycentric interpolation as shown in Fig. 7(d) which is very close to the accurate values as shown in Fig. 7(e). With more sample points, the estimation for the entire space will be more accurate. Based on this idea, in the next section, a new approach is proposed to effectively optimize the dynamic var sources using Voronoi diagram.

V. Proposed Approach

As discussed in Section IV, the Voronoi diagram and Barycentric interpolation are useful techniques to establish function approximation by means of sample points added to the solution space. However, toward the global optimization, without any heuristic information, the Voronoi diagram based blending of local function expression may require many iterations of adding new sample points. Our previous work in

[13] shows that a heuristic LP based method can correctly identify an effective searching direction from an existing point in the solution space, but may jump out of the feasible solution region or converge to the local optimal when the nonlinearity of the optimization problem is significant with four or more dynamic var sources needed to be optimized.

To take the advantage of the Voronoi diagram method on exploring the geometric information on the solution space and the simplicity and time performance of LP in optimization, this section introduces a new approach based on the Voronoi diagram method integrating LP. In each iteration of the approach, Voronoi diagram and Barycentric interpolation are used to identify the most promising region, which integrate LP for determining the search direction to add new sample points without jumping out of that region.

A. Proposed Algorithm

Specifically, this paper proposes the following approach for solving the optimal sizing problem:

Step 1 In the $|I_Q|$-dimensional solution space about Q_i ($i \in I_Q$), i.e. the sizes of placed dynamic var sources, randomly select a set of sample points, denoted by M, and evaluate cost function J_2 about Q_i ($i \in I_Q$) at each point.

Step 2 Establish the Voronoi diagram using all M sample points and estimate the approximate value of J_2 in a neighborhood of each point by Barycentric interpolation.

Step 3 Find the point with the minimal J_2 as a tentative solution.

Step 4 Add three new sample points (as explained in subsections V.B-C), and go back to *Step 2*.

The algorithm can be terminated either after a pre-defined large number of iterations from *Step 2* to *Step 4*, or when the decrease in J_2 is less than a pre-defined tolerance ε.

Fig. 8 illustrates the implementation of the entire approach by integrating the proposed algorithm with power system time-domain simulation. The Voronoi diagram and LP are implemented in MATLAB and are interfaced with power system dynamic simulation software PSS/E via Python. PSS/E solves the DAEs in (4)–(5) to simulate the post-fault voltage responses for any given sizing strategy Q, i.e. a sample point in the solution space. The results are used to evaluate J2 for the strategy and fed back to the Voronoi diagram and LP for function approximation and searching direction identification.

The $|I_Q|$-dimensional space requires at least $|I_Q|+1$ points to establish a Voronoi diagram. To make the diagram authentically present geometrical characteristics of the space, more points should be utilized [19]. In this paper, $2(|I_Q|+1)$ initial sample points are randomly selected in the solution space together with its $2^{|I_Q|}$ geometric vertices (i.e. the limits in all dimensions) to build the first Voronoi diagram.

To improve the fidelity of the global approximation, three new sample points are added every time as *Step 4* is executed: the first point is based on LP to enhance the current tentative optimum within the identified candidate optimum region, the second is to improve the global approximation fidelity at the most depopulated region, and the third is to connect the above two avoiding distorting the Voronoi diagram.

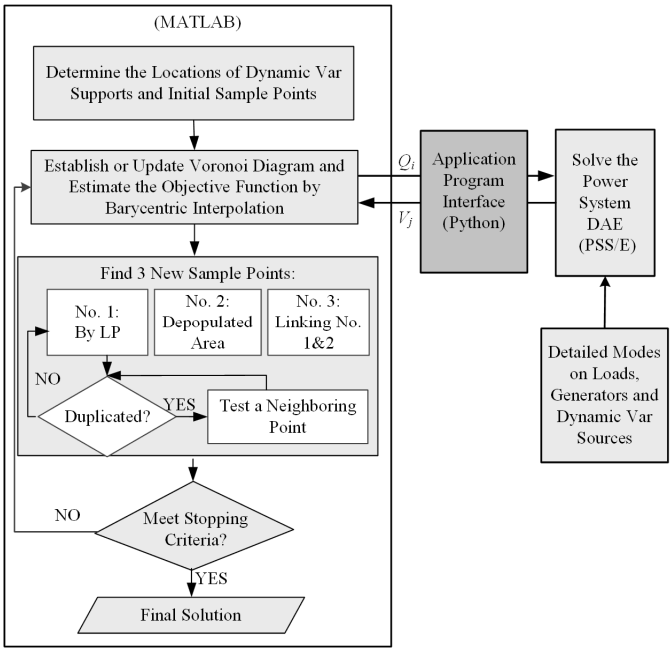

Fig. 8. Flow chart for implementing the proposed approach.

In the following, how to add three new sample points in *Step 4* is introduced in detail.

B. No. 1 New Point by LP for Tentative Optimum Fidelity

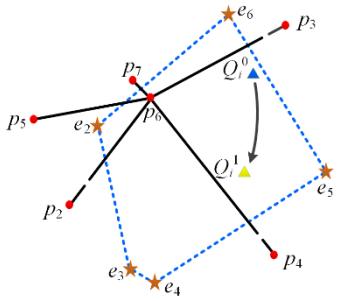

Fig. 9. Addition of a new sample point for the optimum.

As shown in Fig. 9, if the tentative optimal solution is obtained as p_6, the Voronoi region, the polyhedra determined by vertices e_2 to e_6 is considered as the most effective area. A new candidate sample point shown as Q_i^0($i \in I_Q$) is chosen at the estimated minimum value of the objective function in this region by using Barycentric interpolation.

Since the interpolation value will be changed by adding other points, a new sample point Q_i^1 ($i \in I_Q$) is refined by an iterative LP algorithm like [13] utilizing the maximum voltage recovery sensitivity defined by

$$VSI_{ij}^k = \frac{\max(V_j^{k,new,t} - V_j^{k,old,t}, t = 1, \cdots, T)}{q_i}, k = 1, \cdots, K \quad (9)$$

where k is the index of the contingency, q_i is the size of a small dynamic var source (simulated by, e.g., SVC) added at bus i, and $V_j^{k,new,t}$ and $V_j^{k,old,t}$ are the voltage magnitudes

respectively with and without that small var source at time t. The LP algorithm determines Q_i^1 from Q_i^0 by these two steps:

1) Time-domain simulation is performed with SVCs of sizes Q_i^0 ($i \in I_Q$) added to the candidate buses. Then, add a small amount q_i ($i \in I_Q$), e.g. Q_i^U /80, is added to each candidate bus and the simulation under the contingency is performed again. Calculate VSI_{ij}^k ($i \in I_Q$) for the voltage responses with and without q_i ($i \in I_Q$).
2) The direction to update Q_i^0 to $Q_i^1=Q_i^0+\Delta Q_i$ is determined by testing VSI_{ij}^k under contingency k. Then, the amount of update ΔQ_i is determined by solving a LP problem which utilizes the voltage responses obtained from 1).

The detailed algorithm in 2) is given below. Define

$$\Delta V_j^{L,k} = \min(V_j^{k,t} - V_j^{L,t}, t = 1, \cdots, T), j = 1, \cdots, N, k = 1, \cdots, K \quad (10)$$

$$\Delta V_j^{U,k} = \min(V_j^{U,t} - V_j^{k,t}, t = 1, \cdots, T), j = 1, \cdots, N, k = 1, \cdots, K \quad (11)$$

where $V_j^{k,t}$ is the voltage of bus j at time t under contingency k, and V_j^L (V_j^L=0.75V_j^{init} if $t<t_s$ or 0.95 V_j^{init}, otherwise), and V_j^U (V_j^U=1.25V_j^{init} if $t<t_s$ or 1.05 V_j^{init}, otherwise) are respectively the lower and upper limits of bus j voltage. The magnitudes of $\Delta V_j^{L,k}$ and $\Delta V_j^{U,k}$ are actually the closest distances from the voltage trajectory to the two limits under contingency k. $\Delta V_j^{L,k}$ ($\Delta V_j^{U,k}$) is positive if the trajectory is above (below) the limit, or negative, otherwise. Then the following LP problem is solved to determine ΔQ_i ($i \in I_Q$).

$$\text{Minimize } f = \sum_{i=1}^{N} c_i Q_i \quad (12)$$

$$\text{Subject to } Q_i^1 = Q_i^0 + \Delta Q_i, \forall i \in I_Q \quad (13)$$

$$-\alpha^k \sum_{i=1}^{|I_Q|} (VSI_{ij}^k)^T \Delta Q_i \le \Delta V_j^{L,k}, \forall i \in I_Q, j = 1, \cdots, N, k = 1, \cdots, K \quad (14)$$

$$\beta^k \sum_{i=1}^{|I_Q|} (VSI_{ij}^k)^T \Delta Q_i \le \Delta V_j^{U,k}, \forall i \in I_Q, j = 1, \cdots, N, k = 1, \cdots, K \quad (15)$$

$$Q_i^1 (i \in I_Q) \in Vor(Q_i^0 (i \in I_Q)) \quad (16)$$

where α^k and β^k are acceleration factors with a default value of 1. The above LP problem can approximately find the minimum var requirement to improve the post-fault voltage performance by pushing the post-fault voltage trajectories close to the lower voltage limit as much as possible. ΔQ_i($i \in I_Q$) are solved to update Q_i^1($i \in I_Q$) for the next iteration. The constraints (14)–(15) are required because the voltage response is expected to stay within the two limits and approach the lower limit to save the total cost. The constraint (16) is also considered in this LP algorithm because the var size has to stay within the most effective searching space which is the Voronoi region of tentative optimum.

C. No. 2 and No. 3 New Points Respectively for Global Fidelity and Connection of the First Two

For the global fidelity purpose, a region where existing sample points are depopulated must be effective. Under the terminology of the Voronoi diagram, each Voronoi point is the farthest point from its surrounding sample points. A second sample point is chosen based on the largest $dis(p_i,e_i)$ and e_i is the candidate new second point. Taking Fig. 9 as an example, since e_4 is the farthest point to any surrounding p points, it will be the second new sample point if needed.

After the first and second sample points are added, the densities of samples around the tentative optima and around the most depopulated one become quite different. In order to connect the parts of both areas, a third sample point is chosen at the middle point of the straight line connecting the first and second samples points.

As a remark on the proposed approach, the use of the Voronoi diagram together with Barycentric interpolation enables effective cost function approximation for the entire solution space: on one hand, the Voronoi diagram identifies a relatively flat local region for the LP to efficiently optimize the solution; on the other hand, the Voronoi diagram adds new sample points to the most depopulated region to address the global approximation fidelity.

VI. Case Studies

The proposed approach is first illustrated on the WSCC 9-bus system in detail and then tested on the NPCC 140-bus system. The simulation time for each contingency is 5 seconds and integration time step is 1/120s. In the case studies, we assume that all c_i=\$1,000/Mvar, c_p=\$300,000/contingency for the WSCC 9-bus system and c_p=\$3,000,000/contingency for the NPCC system. All buses in one system have the identical penalty for any voltage violation.

A. SVC and Load Modeling

Dynamic models of the dynamic var sources and loads are important for credibly simulating the phenomena of FIDVR and the performance of dynamic var supporting. In case studies, each SVC adopts the PSS/E CSVGN5 SVC model and each load is represented by the PSS/E CLODBL load model [20]. In the following, the SVC and load models will be briefly introduced. For more details on the parameter settings and the functions of the models, please see [20].

TABLE I
PARAMETERS FOR THE SVC MODEL [20]

Parameter	Range	Value
T_{S1}, Filter Lag Time Constant/s	<0.4	0
V_{EMAX}, Voltage Error Max./pu	<0.3	0.15
T_{S2}, 1st Stage Lead Time Constant/s	<2	0.1
T_{S3}, 1st Stage Lag Time Constant/s	(0, 5)	4.5
T_{S4}, 2nd Stage Lead Time Constant/s	<2	0
T_{S5}, 2nd Stage Lag Time Constant/s	<5	0
K_{SVS}, Gain	(50, 1000)	50
K_{SD}, Time Constant/s	(0, 1000)	0
B_{MAX}, Max. Susceptance of SVC/pu	(0,10)	1
B'_{MAX}, Threshold Upper Limit/pu	< B_{MAX}	0.9
B'_{MIN}, Threshold Lower Limit/pu	>-2 B_{MAX}	-0.9
B_{MIN}, Min. Susceptance of SVC/pu	< B'_{MIN}	-1
T_{S6}, Thyristor Delay/s	(2Δt, 0.2)	0.05
DV, Deviation Voltage/pu	(0, 0.5)	0.15

The PSS/E SVC model CSVGN5 is represented as a generator in the power flow model with features including

remote bus voltage control and a fast override capability. Main parameters used in case studies are listed in the first column of Table I. Suggested ranges of their values are provided in the second column and the values adopted in case studies are given in the third column. The control blocks and voltage control characteristics of the SVC are shown in Fig. 10 and Fig. 11. The fast override function in Fig. 10 is activated when the voltage error exceeds a threshold value DV during a fault near the SVC to make the SVC act as a capacitor or reactor. Otherwise, the SVC behaves following the slope K_{SVS} shown in Fig. 11. The MBASE in Fig. 10 is the Mvar output of the SVC and takes the optimized size for this SVC.

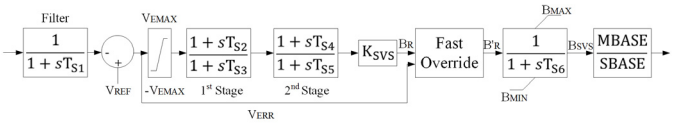

Fig. 10. Control blocks of the CSVGN5 SVC model [20].

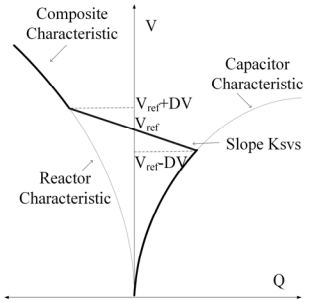

Fig. 11. Voltage-reactive power characteristic of CSVGN5 SVC [20].

As a composite load model, the CLODBL contains large induction motors (LMs), small induction motors (SMs), discharge lighting, distribution transformers with saturation effects, and other static load components as shown in Fig. 12. All load components are assumed to be connected at 0.98 pu voltage. Table II lists the parameters used in case studies.

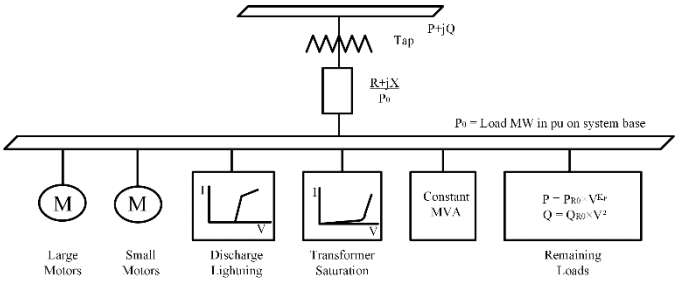

Fig. 12. CLOBDL load model.

TABLE II
PARAMETERS FOR THE COMPOSITE LOAD MODEL

Parameter	Value
Large Motor/%	25
Small Motor/%	25
Transformer Exciting Current/%	3
Discharge Lighting/%	0
Constant Power/%	0
K_p	0.5
R, branch resistance	0
X, branch reactance	0.1

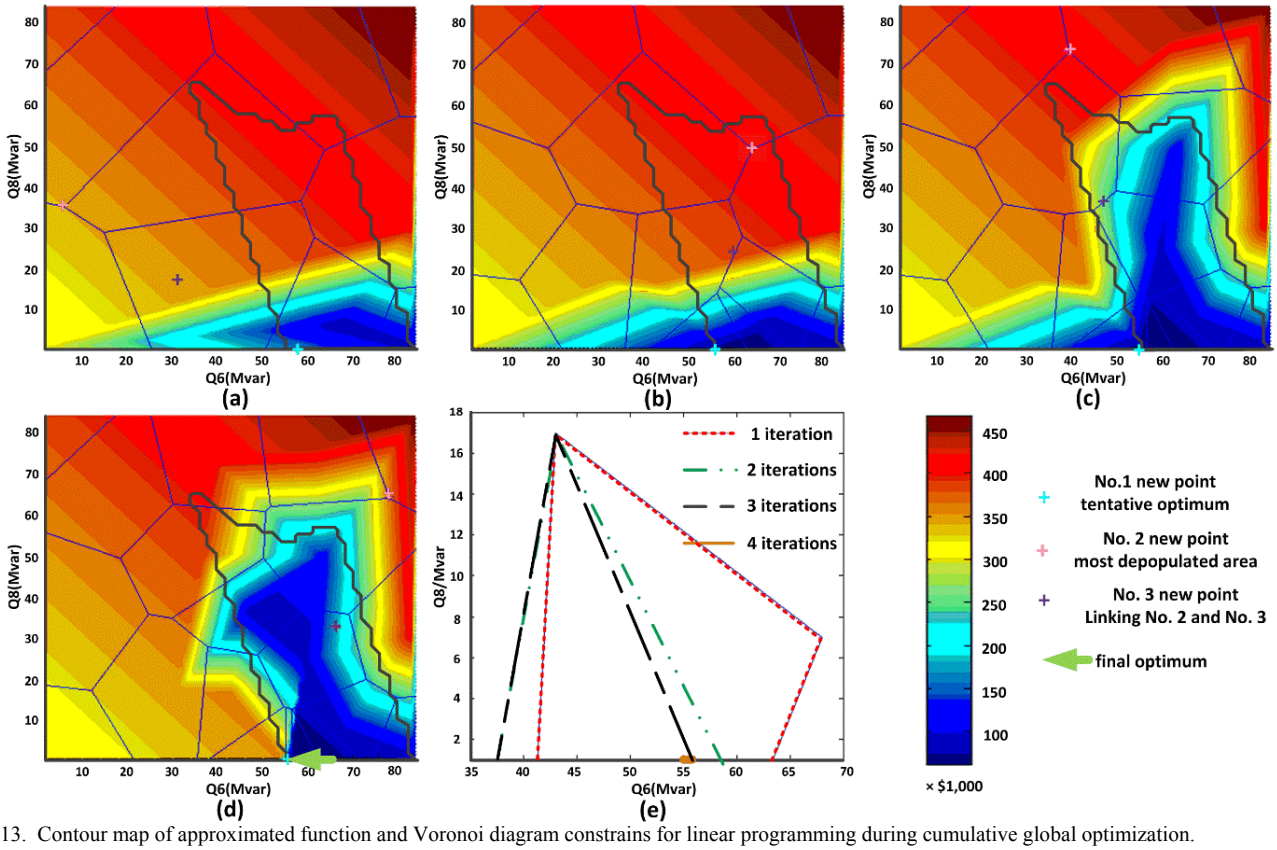

Fig. 13. Contour map of approximated function and Voronoi diagram constrains for linear programming during cumulative global optimization.

B. WSCC 9-Bus System

To illustrate the proposed Voronoi diagram based approach, optimization of the sizes of 2 SVCs at bus 6 and bus 8 is considered. The tolerance in the stopping criterion of iterations is ε=\$1000. The global optimum is found after 3 iterations. Fig. 13 shows the progress of a contour map on the objective function updated with the addition of new samples and how the tentative optimal solution approaches to the actual global optimum. All tentative optimal solutions are checked by the dark solid curves in Fig. 13(a-d) which indicate the boundary of actual feasible solution. Fig. 13(e) illustrates the Voronoi boundary of the tentative optimum in each searching iteration.

Fig. 13(a) gives the initial solution with f=\$75,000 at (Q_6=68Mvar, Q_8=7Mvar) under the initial approximation with 10 sample points. In Fig. 13(b), the solution is updated to f=\$59,000 at (Q_6=58Mvar, Q_8=1Mvar) with 13 sample points after the first iteration. In Fig. 13(c), the tentative solution is moved to f=\$57,000 at (Q_6=56Mvar, Q_8=1Mvar). In Fig. 13(d), the shapes of the cost function in polygons are further refined specifically for the areas around the true optimum, and the global optimal solution as indicated by the arrow has f=\$57,000 at (Q_6=56Mvar, Q_8=1Mvar). The solution obtained from the proposed approach is verified to be the same as the global optimum found by exhaustive search.

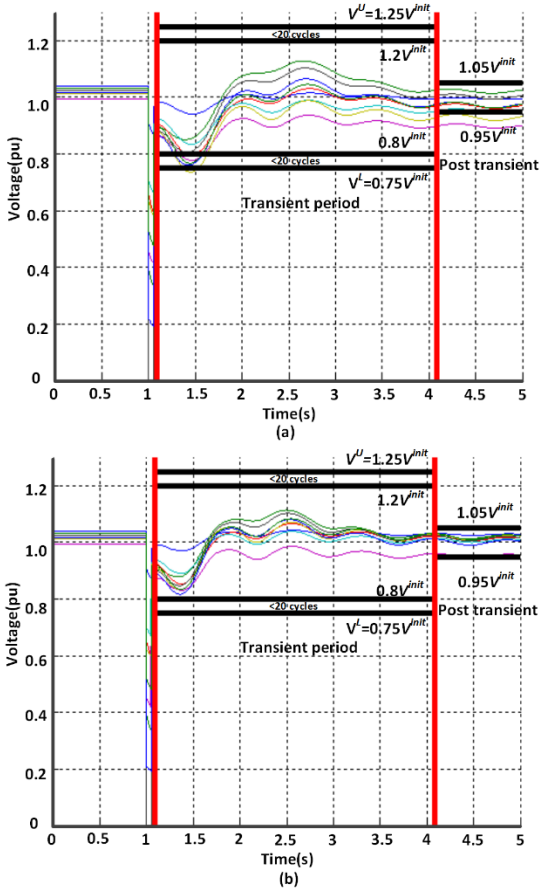

Fig. 14. Post-fault voltage responses of WSCC system.

Fig. 14 illustrates bus voltage profiles in time domain without and with the optimal dynamic var supporting. In Fig. 14(a), FIDVR is seen on the voltage trajectories of 5 out of 9 buses without any var support. During the transient period, one load bus violates C_1, i.e. the 75% of initial voltage lower limit, and four buses violate C_2, i.e. the voltage duration between 75% and 80% of the initial voltage longer than 20 cycles. Also, at the post transient period, two buses violate C_3, i.e. the 5% deviation limit. The severity index S^k of the system under this contingency is 0.0079 pu. Fig. 14(b) shows all of voltage trajectories meet the voltage criteria with the optimally sized SVCs, indicating a severity index of zero.

C. NPCC System

The proposed approach is also tested on the NPCC 48-generator 140-bus system as shown in Fig. 15, which represents a simplified equivalent of the northeast region of the Easter Interconnection power grid. Consider 7 SVCs to be installed at seven predetermined buses 3, 6, 7, 12, 16, 34, and 56, which are optimized by the empirical controllability covariance based fault specified method in [6], to mitigate the FIDVR issues under the most severe "N-1" contingency. Assume that the size of each SVC ranges from 0 to 400 Mvar. The tolerance in the stopping criterion of iterations is ε=\$5000.

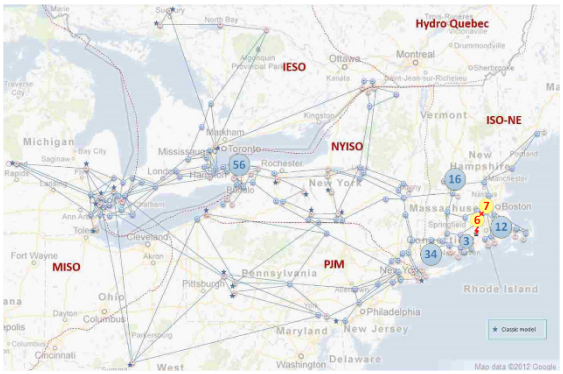

Fig. 15. NPCC system and the most severe N-1 contingency and seven candidate buses for dynamic var sources (important buses are highlighted in the following discussion).

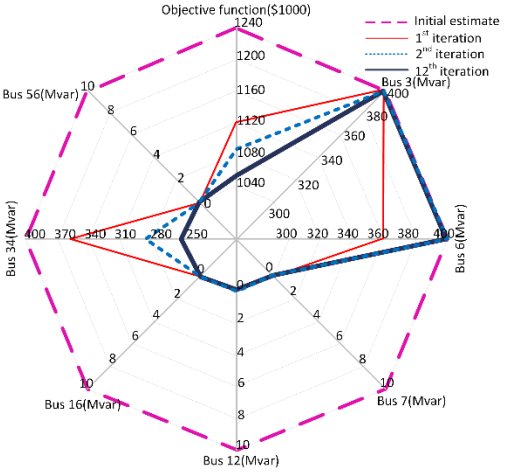

Fig. 16. Searching path of the optimization of dynamic var on the NPCC system under the most severe N-1 contingency.

The most severe "N-1" contingency is identified to be the outage of line 6–7 by a three-phase-to-ground fault on bus 6 with 5-cycle clearing time. Starting an initial estimate based on $2\times(7+1)=16$ initial sample points and $2^7=128$ geometric vertices, the approach adds three new points for each iteration. Fig.16 shows the trajectory of iterations converging to an optimum in the spider chart. The initial estimate of optimum f=\$1,240,000 is at (400, 400, 10, 10, 10, 400, 10) in the space about Q_3, Q_6, Q_7, Q_{12}, Q_{16}, Q_{34}, and Q_{56}. After the first iteration, the tentative optimum is found to be f=\$1,120,000 with the Q_3=400Mvar, Q_6=Q_{34}=360Mvar, and others to be 0Mvar. Finally, after 12 iterations, the search stops at an optimum having f=\$1,055,000 with Q_3=Q_6=400Mvar, Q_{34}=255Mvar, and others 0 Mvar. An exhaustive search is performed in the seven-dimensional solution space and that obtained solution after 12 iterations is verified to be the true global optimum.

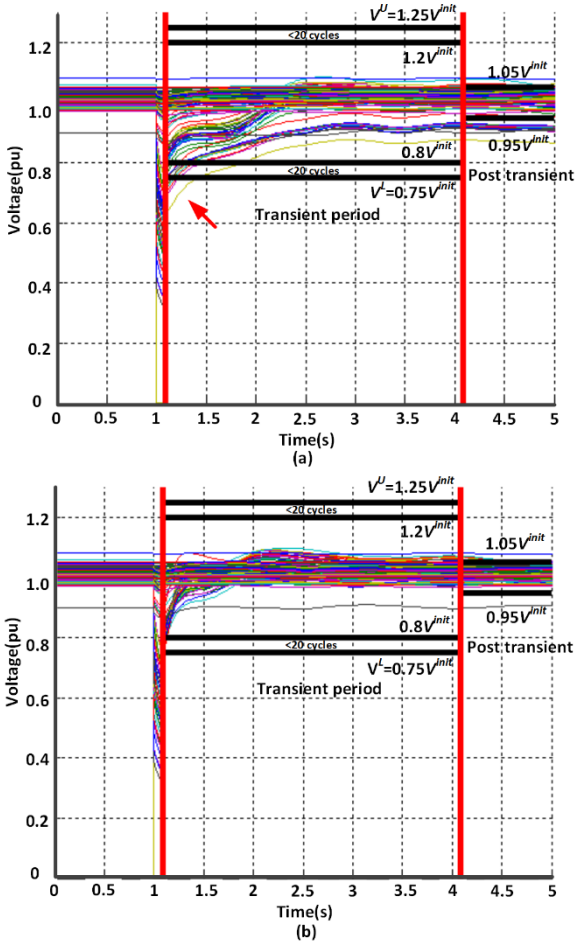

Fig. 17. Post-fault voltage responses of NPCC most severe N-1 system.

Fig. 17 illustrates bus voltage profiles in time domain simulation without and with the optimal SVC support. In Fig. 17(a) shows the delayed voltage recovery phenomenon without any var support in which 5 buses violate C_1 at the beginning of the 3-second transient period and some buses violate C_3 in the post transient period, the severity index S^k for the contingency without any var support is 0.0034 pu and the network loss is 1.3356% of the total system load. Fig. 17(b) shows the all of voltage trajectories meet the voltage criteria with the obtained optimal sizes of SVCs, the severity index becomes zero with optimized var support and the network loss slightly reduces to 1.3267% of the total system load.

Consider the same critical contingency but change the percentages of both LMs and SMs loads from 25% to 22.5%, 20%, and 17.5%, respectively, in order to investigate the impacts from variations in the level of dynamic load. The optimal sizes of seven SVCs for four different percentages of motor loads are listed in Table III and visualized by the spider chart of Fig. 18. From Fig. 18, the spider of the solution about the load model with a smaller percentage of motors is always inside the spider with a larger percentage of motors. It indicates that the SVCs whose sizes are optimized for a certain percentage of motor loads can still address the FIDVR issue with the critical contingency when that percentage decreases. In practice, it is not economical to optimize sizes of dynamic var sources considering many levels of dynamic load and all possible loading conditions. Also, considering the observation from Fig. 6 that the optimal solution for a heavy-load condition remains its feasibility for a light-load condition, an advisable strategy is to consider the peak load condition with a large enough percentage of motor loads in the simulation and optimization of dynamic var sources.

TABLE III
IMPACT OF DIFFERENT PERCENTAGES OF MOTOR LOAD

LM/%	SM/%	Optimized Var Sizes/Mvar [Q_3, Q_6, Q_7, Q_{12}, Q_{16}, Q_{34}, Q_{56}]
25	25	[400, 400, 0, 0, 0, 255, 0]
22.5	22.5	[395, 400, 0, 0, 0, 5, 0]
20	20	[230, 400, 0, 0, 0, 0, 0]
17.5	17.5	[50, 400, 0, 0, 0, 0, 0]

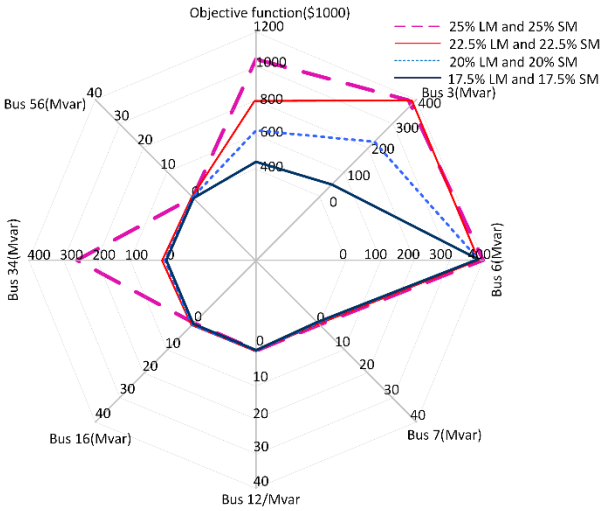

Fig. 18. Optimal sizes of dynamic var sources under different load condition.

Additionally, the sensitivity of the proposed approach is to the set of initial sample points is tested on optimizing 5, 6, and 7 SVCs. Besides the initial $2(|I_Q|+1)$ random sample points plus $2^{|I_Q|}$ geometric vertices, each iteration adds 3 new sample points based on the rules in Section V.B–C. For each test case,

five independent tests are performed in order to find the average performance of the approach. Each test starts from $2(|I_Q|+1)$ random initial sample points followed by $2^{|I_Q|}$ geometric vertices and then adds 3 new sample points per iteration. For each test, a large number of iterations are performed to observe the convergence performance of the approach. All tests model each load bus with 25% LMs load and 25% SMs load. The best locations of SVCs are determined by the method in [6]. The environment to test time performance of the approach is a desktop computer with 3.6 GHz I7-4790 CPU and 16 GB RAM.

For 5 SVCs, they are placed at buses 3, 6, 12, 19, and 30. Each test starts from $2\times(5+1)=12$ initial sample points and $2^5=32$ geometric vertices. From the Fig. 19, after only 8 iterations, all tests converge to the total cost of $1,175,000 with an optimum at (400, 400, 0, 0, 375) about Q_3, Q_6, Q_{12}, Q_{19}, and Q_{30}, respectively.

For 6 SVCs, they are placed at buses 3, 6, 7, 12, 34, and 56. Each test starts from $2\times(6+1)=14$ initial sample points and $2^6=64$ geometric vertices. From Fig. 20, after 12 iterations, all tests converge to the total cost of $1,055,000 at (400, 400, 0, 0, 0, 255, 0) about Q_3, Q_6, Q_7, Q_{12}, Q_{34}, and Q_{56}.

For the tests on 7 SVCs, starting with $2\times(7+1)=16$ initial sample points and $2^7=128$ geometric vertices, the approach takes 15 iterations to have all tests converge to the optimum, as shown in Fig. 21.

The above tests show that the proposed approach quickly converges to the optimum after iterations of a moderate number, which is not sensitive to the selection of initial sample points.

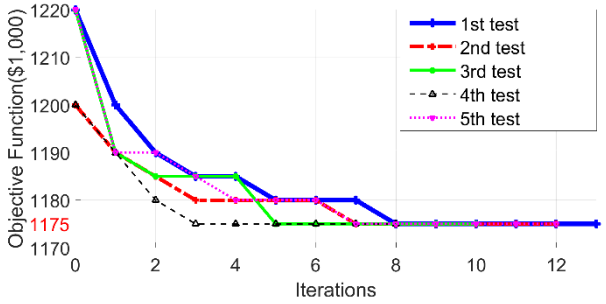

Fig. 19. The process of the proposed approach with 5 independent tests for installing 5 SVCs

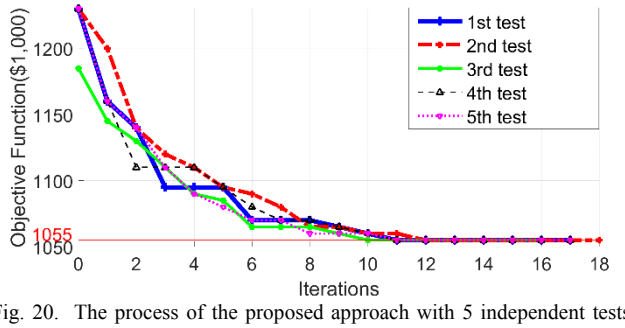

Fig. 20. The process of the proposed approach with 5 independent tests for installing 6 SVCs

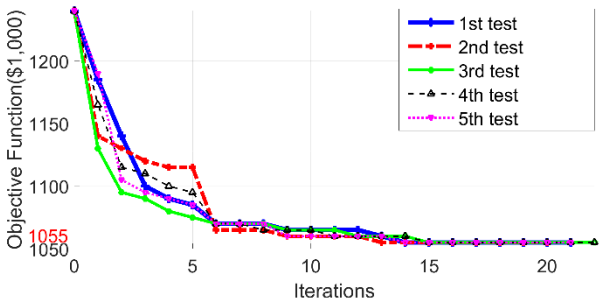

Fig. 21. The process of the proposed approach with 5 independent tests for installing 7 SVCs

For the tests above on optimizing 5, 6, and 7 SVCs, Table IV gives the time performances of the proposed approach. The initial stage on $2(|I_Q|+1)+2^{|I_Q|}$ points takes respectively 439 s, 778 s and 1436 s, which each include the times for the time-domain simulation in PSS/E and the cost function calculation on initial sample points and creation of the initial Voronoi diagram in MATLAB. The time cost per point is about 10s. The iteration stage takes 728 s, 1320 s, and 1980 s, respectively for 8, 12, and 15 iterations, i.e. the worst one among five tests. The time costs on one iteration are 91 s, 110 s, and 132 s, respectively, each including the times for evaluating 3 new points, LP, and updating the Voronoi diagram.

TABLE IV
TIME PERFORMANCE

No. of SVCs	Initial stage time cost on $2(\|I_Q\|+1)+2^{\|I_Q\|}$ points (s)	Iteration stage time cost (s)	Total time (s)
5	439	91×8=728	1167
6	778	110×12=1320	2098
7	1436	132×15=1980	3416

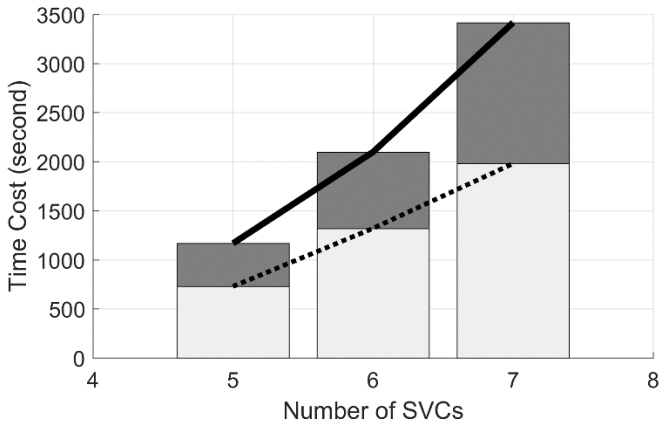

Fig. 22. Time costs for optimizing 5, 6 and 7 SVCs

Fig. 22 depicts the bar chart and the trends on the total time costs, where the light and dark regions of each bar respectively represent the time costs on the initial stage and on the iteration stage. The total time cost will grow exponentially with the increase of the number of dynamic var sources. This approach can be applied offline to solve the optimal sizing problem in the planning stage. In practice, the total number of dynamic var sources, e.g. SVCs and STATCOMs, needed by an electric

utility company is not large (typically, <10), and if necessary, high-performance computers may be applied to solve the problem in a faster manner.

VII. Conclusion

This paper proposes a new approach for solving optimal sizes of dynamic var sources against the FIDVR issues. That is of a complex non-convex optimization problem. The geometric characteristics about the non-convex solution space of this problem has been studied. Accordingly, a Voronoi diagram based approach integrating LP was proposed and illustrated on the WSCC 9-bus system by case studies. The approach was also validated on the NPCC 140-bus system to quickly give the optimal sizes of seven SVCs against the most severe "N-1" contingency.

References

[1] A. Tiwari and V. Ajjarapu, "Addressing short term voltage stability problem – Part I: Challenges and plausible solution directions," *IEEE PES T&D*, pp. 1–5, May 2016.

[2] A. Tiwari and V. Ajjarapu, "Addressing short term voltage stability problem – Part II: Case study," *IEEE PES T&D*, pp. 1–5, May 2016.

[3] S. A. Meliopoulos, V. Vittal, J. McCalley, V. Ajjarapu, I. Hiskens, et. al., "Optimal allocation of static and dynamic VAR resources", *Final Report to Power Systems Engineering Research Center (PSERC)*, Mar. 2008.

[4] B. Sapkota and V. Vittal, "Dynamic Var planning in a large power system using trajectory sensitivities," *IEEE Trans. Power Syst.*, vol. 25, no. 1, pp. 461–469, Feb. 2010.

[5] V. Krishnan, H. Liu, and J. McCalley. "Coordinated reactive power planning against power system voltage instability," *IEEE/PES Power Systems Conference and Exposition*, Seattle, WA, Mar. 2009.

[6] J. Qi, W. Huang, K. Sun, and W. Kang, "Optimal placement of dynamic var sources by using empirical controllability covariance", *IEEE Trans. Power Syst.*, vol. 32, no. 1, pp. 240–249, Jan. 2017.

[7] A. Tiwari and V. Ajjarapu, "Optimal allocation of dynamic VAR support using mixed integer dynamic optimization," *IEEE Trans. Power Syst.*, vol. 26, no. 1, pp. 305–314, Feb. 2011.

[8] M. Paramasivam, A. Salloum, V. Ajjarapu, V. Vittal, N. B. Bhatt, and S. Liu, "Dynamic optimization based reactive power planning to mitigate slow voltage recovery and short term voltage instability," *IEEE Trans. Power Syst.*, vol. 28, no. 1, pp. 3865–3873, Nov. 2013.

[9] Y. Xu, Z. Dong, K. Meng, W. Yao, R. Zhang, and K. Wong, "Multiple-objective dynamic var planning against short-term voltage instability using a decomposition-based evolutionary algorithm," *IEEE Trans. Power Syst.*, vol. 29, no. 6, pp. 2813–2822, Nov. 2014.

[10] S. Wildenhues, J. Rueda, and I. Erlich, "Optimal allocation and sizing of dynamic var sources using heuristic optimization", *IEEE Trans. Power Syst.*, vol. 30, no. 5, pp. 2538–2546, Sept. 2015.

[11] H. Liu, V. Krishnan, J. D. McCalley, and A. Chowdhury, "Optimal planning of static and dynamic reactive power resources," *IET Gener. Transm. Distrib.*, vol. 8, no. 12, pp. 1916–1927, 2014.

[12] Z. Hussain, Z. Chen, P. Thogersen, and P. Lund, "Dynamic reactive power compensation of large-scale wind integrated power system", *IEEE Trans. Power Syst.*, vol. 30, no. 5, pp. 2516–2526, Sept. 2015.

[13] W. Huang, K. Sun, J. Qi, and Y. Xu, "A new approach to optimization of dynamic reactive power sources addressing FIDVR issues," *IEEE PES General Meeting*, National Harbor, MD, 2014.

[14] W. Huang, K. Sun, J. Qi, and Y. Xu, "Voronoi diagram based optimization of dynamic reactive power sources," *IEEE PES General Meeting*, Denver, CO, 2015.

[15] M. G. O. Cheong, et al, *Computational Geometry: algorithms and applications* (3rd ed.), Springer-Verlag, New York, 2008.

[16] D. J. Shoup, J. J. Paserba, and C. W. Taylor, "A survey of current practices for transient voltage dip/sag criteria related to power system stability," *IEEE PES PSCE.* Oct. 2004.

[17] NERC/WECC Planning Standards, WECC, Apr. 2003.

[18] N. Hirokawa, K. Fujita, and T. Iwase, "Voronoi diagram based blending of quadratic response surfaces for cumulative global optimization", *9th AIAA/ISSMO Symposium on Multi-Disciplinary Analysis and Optimization,* Atlanta, GA, Sept. 4–6 , 2002.

[19] S. Cheng, T. K. Dey, and J. R. Shewchuk, *Delaunay Mesh Generation,* CRC press, Jan., 2013.

[20] Siemens PTI Power Technologies Inc., PSS/E 33, Program Application Guide, vol. II, May 2011.

Biographies

Weihong Huang (S'14) received the B.E degree from Huazhong University of Science and Technology, Wuhan, China, in 2009, and the master degree from University of Tennessee, Knoxville, TN, USA in 2014, both in electrical engineering. She worked at Yueqing Electric Power Bureau, Grid State Corporation of China, Wenzhou, China, from 2009 to 2012. Currently, she is pursuing her Ph.D. degree at Department of EECS, University of Tennessee, Knoxville, TN, USA. Her research interests include planning and control of reactive power and model validation.

Kai Sun (M'06–SM'13) received the B.S. degree in automation in 1999 and the Ph.D. degree in control science and engineering in 2004 both from Tsinghua University, Beijing, China. He is currently an assistant professor at the Department of EECS, University of Tennessee in Knoxville. He was a project manager in grid operations and planning at EPRI, Palo Alto, CA from 2007 to 2012. Dr. Sun is an editor of IEEE Transactions on Smart Grid and an associate editor of IET Generation, Transmission and Distribution. His research interests include dynamics, stability and control of power systems and other complex network systems.

Junjian Qi (S'12–M'13) received the B.E. and Ph.D. degrees, both in electrical engineering, from Shandong University, Jinan, China, in 2008 and Tsinghua University, Beijing, China, in 2013, respectively. Dr. Qi is currently a Postdoctoral Appointee at the Energy Systems Division, Argonne National Laboratory, Argonne, IL, USA and a joint appointed Argonne Staff at the Computation Institute, University of Chicago, Chicago, IL. He was a visiting scholar at Iowa State University, Ames, IA in February–August 2012, and a Research Associate at the Department of EECS, University of Tennessee, Knoxville, TN in September 2013–January 2015. Dr. Qi is the Secretary of the IEEE Task Force on "Voltage Control for Smart Grids". His research interests include cascading blackouts, power system dynamics, state estimation, synchrophasors, voltage control, and cybersecurity.

Jiaxin Ning (S'07–M'10) was graduated from Chongqing University, China with B.S. and M.S of Electrical Engineering Degrees in 2004 and 2007, respectively. In 2010, he received his Ph.D. degree in Electrical Engineering from Tennessee Technological University, Tennessee, USA. Dr. Ning is currently with Dominion Virginia Power for transmission planning and strategic initiatives. His responsibility covers transmission network planning and design, generation interconnection, generator stability and special protection, dynamic voltage and reactive power control, implementation of FERC Order 1000 to mitigate PJM's congestion, etc. Before joining Dominion Virginia Power in 2014, Dr. Ning worked in EnerNex LLC, Knoxville, Tennessee, as a senior consultant to initiate and lead industrial and research projects.